Correlation Analysis of Ultrasonic Stress Wave Characteristics and the Destructive Strength Measurements in Cylindrical Wooden Structure

Yishi Lee, Frederico Nistal Franca, R. Daniel Seale, Jerrold E. Winandy, and Christopher A. Senalik

Abstract—**Ultrasonic-based nondestructive evaluation (NDE) has been employed in the utility sector to determine the cross-sectional groundline integrity of wooden utility poles. While it is far less invasive than other methods, its efficacy has not been thoroughly examined. This study aims to fill this technical gap by analyzing the correlation between the propagational characteristics of the ultrasonic stress wave using a novel embedded waveguide technique and the existing destructive testing methods. The proposed embedded waveguide technique excites diffusive Rayleigh mode (AW2) propagates in the shell region of the cross-sectional plane. The employed Gabor wavelet transformation and the model-based arrival region identification extract the propagation velocity and the associated spectral response of AW2. This study uses the static break assessment per ASTM 1036 Standard Test Methods and the longitudinal compression test per ASTM D143–14 "secondary method" to quantify the cross-sectional strength of the test specimen. This work performs a comprehensive correlation analysis between the extracted AW2 features and the associated destructive test. An overall correlation R^2 from 0.2 to 0.5 is achieved between the AW2 features and the static break test results. An overall correlation of R^2 of 0.4 is achieved for 30 to 35-foot poles in the longitudinal compression test.**

Index Terms—**Wave Propagation (including elastic waves), Industrial Measurement and Control, Signal and Image Processing, wooden utility poles, Material & Defect Characterization.**

I. Introduction

The United States power and communication infrastructure relies on the structural integrity of approximately 154 million wooden utility poles. A reliable structural monitoring system is vital to ensure the sustainability of these networks. The traditional evaluation process has mainly relied on partial excavation, sound and bore techniques but the invasive nature can inadvertently damage the previously established internal chemical and physical characteristics of the poles. A recent study conducted by J. Winandy reveals that any incision in the wooden surface could negatively affect the strength in the cross-sectional plane [1]. Additionally, the ANSI specification for new poles [2] prohibits open or plugged holes. A number of comparison studies by U.S. utilities have indicated that ultrasonic nondestructive testing (NDT) can produce the same level of efficacy as the partial excavate, sound and bore process. However, the correlation between ultrasonic NDT and the destructive testing has not been academically evaluated. This study aims to fill gaps in this area by comparing an ultrasonic method with the destructive evaluation methods [3] and [4].

The problem of Ultrasonic stress waves in wood was first examined by [5]. Previous studies from [6], [7] and [8] have significant contributions in this area. The associated theoretical and numerical models have also been developed to understand the stress wave propagational mechanism [9], [10] and [11]. J. Winandy and J. Morrell evaluated the efficacy of ultrasonic inspection of progressively decayed wood in 1993 [12]. They have concluded that using time-of-flight (TOF) as a sole metric for wood characterization might appear unreliable [12]. In 1992, Bucur and Feeney pioneered the study of the energy interactions with the dispersive medium [13]. Due to the complex wave interactions within the medium, various attempts have been conducted to extract features in the received signal that can improve the characterization of the physical properties of the medium. That includes time centroid measurements [14], signal attenuation by using root-mean-square (RMS) [15], and fuzzy logic [16]. [17] and [18] incorporated the findings from the elastodynamic formulation into the signal analysis process, effectively dissected the waveform according to different arrivals. Using time-frequency domain representation, critical parameters of a reflected stress wave can be extracted to characterize the material property. A recent study by [19] performed a thorough analysis by formulating a multivariable linear regression (MLR) as a function of reflected signal parameters and known material properties to estimate the ultimate tensile strength (UTS)
.

This study begins with the ultrasonic test by acquiring the through-transmission stress wave signal using the UB1000 device. The ultrasonic test is performed in the cross-sectional planes from 1 foot below grade up to 4

Y. Lee is with the Department of Engineering and Engineering Technology at Metropolitan State University of Denver, Denver, CO, 80128 USA e-mail: ylee24@msudenver.edu.

F. N. Franca and R. Daniel Seale are with the College of Forest Resources at the Mississippi State University, Mississippi State University, Mississippi State, MS 39762.

J. Winandy is with the Winandy & Associates LLC, Ham Lake, MN, 55304.

C. Senalik is with the USDA Forest Products Laboratory, Madison, WI, 53726

feet above grades with a 1-foot longitudinal increment. The details of the process are described in Section II-A. The associated physics-based signal analysis technique of extracting vital information from the stress wave signal is explained in Section II-B. The poles are then subjected to the static break test in accordance with the ASTM 1036 Standard Test Method. The setup and the system of performing static mechanical testing are discussed in Section II-C. The poles are then cut to a specific length in the longitudinal direction for the longitudinal compression testing. The procedures are detailed in Section II-D. The results from the mechanical testing (static break test and the compression test) are examined against the stress wave signal with the detailed analysis provided in Section III. Fig. 1 illustrates the test sequence and the associated correlation analysis.

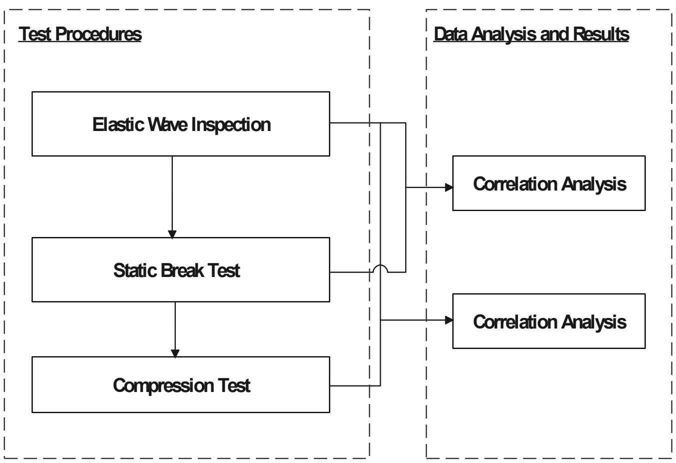

Fig. 1. Sequence of the Test and the proposed analysis approach

II. Methodology and Experimental Setup

A. Through-Transmission Mode

The sectional plane above grade is first determined. An arbitrary 0-180 degree is chosen as the reference points in this sectional plane (See Fig. 2a). Two embedded waveguides are inserted 15 mm into the medium. The same procedure is repeated for the 90-270 orientation. It is observed that the two orientations can produce vastly different responses. This phenomenon is primarily due to the orientation of the local imperfection in the sectional plane with respect to the direction of the traveling stress field. When the lengthwise direction of the imperfection is perpendicular to the propagation direction, strong reflection can occur, causing interference response and stronger attenuation at the receiving end. Likewise, when the lengthwise direction of imperfection is parallel to the propagation direction, the interaction is much weaker. This process is illustrated in Fig. 2b. Hence, the drastic difference in signals between the two orthogonal directions is an indication of a local imperfection. In this study, two orientations are compared, and the highest signal-to-noise (SNR) is selected for analysis. When both orientations result in similar energy and temporal responses, it is often an indication of a global response of the sectional plane in question.

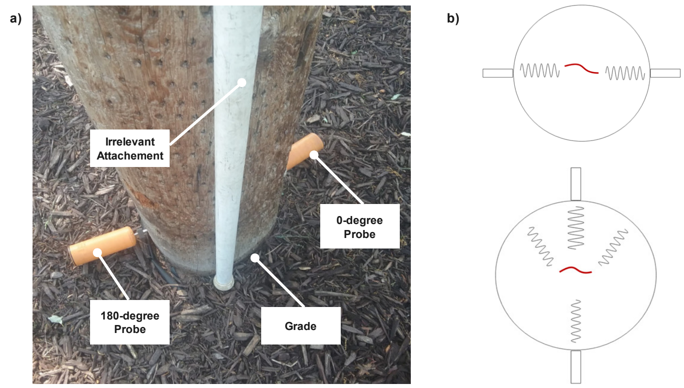

Fig. 2. Test for the sectional plane, b) Orientation of localized Defect and plane wave response

B. Characteristics of Rayleigh Mode Response

Stress wave in this study is produced by an acoustic device (UB1000) [20] designed to generate a narrow-band radiation source of 50 kHz utilizing a high power piezoelectric transducer. Custom circuitry in the probe produces high voltage discharge, and processes received the analog signal using an onboard analog-to-digital unit. The device is coupled to an embedded waveguide inserted into the wooden medium to produce radial and circumferential Rayleigh modes [11]. Previous study by [17] has concluded that the velocity and diffusive characteristics of the circumferential Rayleigh mode or the *arrival mode number 2* (AW2) can characterize the material properties near the half-space boundary. Through the semi-explicit differential-algebraic equation representation of Navier's equation, [21] has discovered that the Rayleigh mode can be extracted from the complex stress wave response in the circular cross-sectional plane of the groundline region. The study produced by [22] has indicated the decay mechanism can contribute to the loss of porosities. Based on M.A. Biot's formulation of poroelastic stress propagation in a multi-phase medium, the viscous damping coefficient of the displacement field depends strongly on the coupling factor [23] and [24], which cause amplitude attenuation of the propagating stress wave. The energy propagation velocity responds strongly to the change of elastic moduli and density [25]. The aggregate findings inspire the use of analytic wavelet to represent the temporal waveform in the time-frequency (TF) domain. This representation extracts the Rayleigh mode arrival along with the energy content.

Wavelet transformation is an inner product defined by the following [26],

$$W_{\psi}^{y}(a,b) = \frac{1}{\sqrt{c_{\psi}|a|}} \int_{-\infty}^{\infty} y(t)\psi\left(\frac{t-b}{a}\right) dt, \qquad (1)$$

where a is the dilation parameter and b is the translation parameter. $y(t)$ is the stationary time signal. ψ is an operator function defined as the mother wavelet. The mother wavelet takes on different forms depending upon the application. To select a proper mother wavelet, prior work by [27] indicates that signal containing dynamic frequency and time components should use analytic wavelet function (AWT) to analyze the signal. Non-analytic mother wavelet often leads to interference and artifacts that can erroneously represent the amplitude and phase. Analytic mother wavelets such as the Gabor, analytic form of the Mexican hat, and Cauchy are considered. The most proper wavelet tends to have a matched shape as the signal in question [28]. Among the examined wavelets, the Gabor wavelet exhibits a temporal response similar to the transient waveform estimation by the dual waveguide configuration. The Gabor wavelet exhibits an acceptable frequency resolution for better spectral analyses and detection of the spectral response in the low-frequency region. Based on the findings from analytical and numerical models [21], the Gabor continuous wavelet transformation (CWT) produces a desirable temporal and spectral representation of the signal to detect the mechanical and the poroelastic variations in the propagating medium. This transformation suffers temporal resolution in that range, but it is a common drawback in any TF domain representation according to the uncertainty principle [29]. Fig. 3 depicts TF representation of time-series Analog-to-digital (ADC) signal. Two pronounced clusters correspond to the energy arrival of AW1 and AW2 arrival regions as illustrated in Fig. 3a. By isolating the fundamental frequency of the received waveform, it yields the energy response in the temporal domain as illustrated in 3b. The peaks that are circled corresponds to the arrivals of dominant energy propagation. The peak value provides both temporal information which can translate to the propagation velocity and the attenuation of the energy. The next section will empirically examine the proposed techniques.

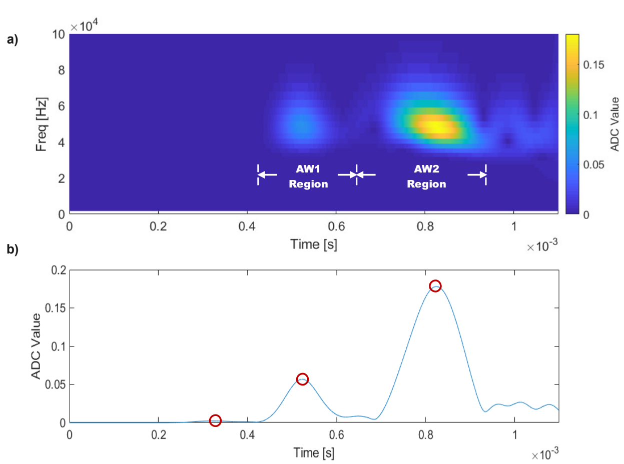

Fig. 3. Arrival regions in the TF domain analysis.

TABLE I
SAMPLE SET FOR I_0 DETERMINATION.

AGL	Cir	ENG of AW2
24	47.72	1015
48	46.88	1499

1) AW2 Average Arrival Velocity: Using the proposed wavelet analysis technique, the extracted temporal-energy response in the signal can be examined. By discarding the effect of intermodal interference, the stress energy of the specific arrival mode dominates the energy contained within the selected arrival region. Hence, this study focuses on the extraction of the peak energy to determine the Rayleigh mode propagation. Since the propagation plane has a dimensional variation based on the pole class and the tapering effect above grade, this variation is considered by computing the average propagating velocity with the corresponding circumference [17] at the plane of propagation. That is,

$$\bar{v}_{pe} = \frac{C_{B,BP}}{t_{pe}}, \tag{2}$$

where $C_{B,BP}$ is the circumference of the propagation plane, t_{pe} is the arrival time at the energy peak.

2) Energy Attenuation Coefficient α_{pe}: In linear viscoelastic solid such as wood, the inelastic scattering and the irreversible process attenuates the energy of the wave. This process can be explained theoretically by analyzing the Biot's formulation and the increase of porosity due to incipient decays [11]. To quantify the attenuation characteristics, peak energy response is used to extract the primary mode and the attenuation can be computed based on the following power-law model. [30].

$$I(\alpha, x) = I_0 e^{-\alpha x}, \tag{3}$$

where I_0 is the initial intensity of the stress wave, I is the energy flux measured in an attenuating medium at a distance x from the source, and α is the attenuation coefficient. The power-law model describes the received energy intensity as a function of the initial wave intensity, propagation distance, and the attenuation coefficient. The attenuation coefficient strongly couples with the property of the medium [11]. In turn, it provides the means to characterize the condition of the medium. By manipulating (3) into the following expression,

$$\alpha_{pe} = \frac{2 \ln I_0 / I}{C_{B,BP}}, \tag{4}$$

where $C_{B,BP}$ is the circumference of the sectional plane in question. I_0 can be determined by obtaining the energy response of an arbitrary pole with AGL at 24 and 48 inches (See Table I). The tapering geometry of a pole generates two simultaneous equations for estimating I_0.

C. Static Break Test

Mechanical testing of wood poles was carried out in accordance with the test requirement and data collection requirement of [3]. Fig. 4b illustrates the actual setup of the test. A test specimen is restrained at the groundline and few inches above the bottom of the pole to simulate the ground support. A cart shown in Fig. 4b supports the tip of the pole to eliminate orthogonal load due to gravity. A tip load is applied 2 feet from the pole's tip using the variable speed winch until reaching the sufficient failure force.

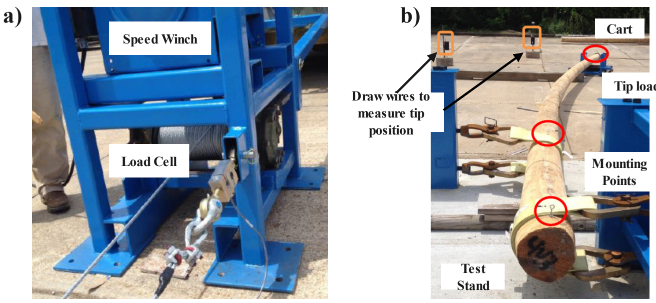

Fig. 4. Setup of the static break test.

To measure the deflection, a system of four draw wire sensors measures the pole deflection. Two draw-wire sensors measure the movement 2 feet from the tip at the point of load application. Two draw-wire sensors measure the rotation or ground-line movement at the butt, allowing the exact measurement of the tip location with respect to the groundline. A load cell (Fig. 4)a is mounted on the speed winch measures half of the applied load.

Based on the applied failure load and the measured deflection, the empirical value of the maximum fiber strength at the groundline can be calculated based on the following equation [31] and [32]:

$$F_b = 32\pi^2 P(a - \Delta a)/C_a^2, \tag{5}$$

where F_b denotes the maximum fiber stress of the location of the *plane of rupture* (POR), P is the imposed failure tip load, a is the longitudinal distance between the load point and the break, and Δa is the maximum longitudinal deflection which is express as, $\Delta a = \Delta_L[1 - (b/L)^3]$.

During the test process, a test specimen is first rested on a test stand and restrained at the predetermined mounting points. Based on the specimen's pole class, the winch placement or the load point is determined in accordance with [33]. Each specimen was tested with a load applied at a constant rate. Simultaneously, the tip position is measured at a 10 Hz sampling rate. Once the testing was completed, the load and deflection measurements are used to determine the modulus of elasticity (MOE) and the modulus of rupture (MOR).

D. Compression Test

Since the rupture plane from the static break test produces an unsuitable surface for the longitudinal compression testing, a 1-foot cylindrical specimen is cut at about one foot from the rupture plane to avoid the alternation of mechanical property. The prepared specimen is stored in a controlled environment with a temperature of 75 ^{0}C, relatively humility of 50 % for 43 days. The compression parallel to the grain procedure was done in accordance with [34]. Using 1-inch by 1-inch square metal rod, the load was applied to the surface of specimens at a rate of 0.1 inches per minute until 0.1 inch is achieved. The load is recorded to calculate the corresponding compression stress. Figure 5 shows the setup of the experiment.

Fig. 5. Setup of the compression test

In order to the average response in both the shell and heart regions, nine different points with 5 positioned in the heart region and 4 positioned in the shell region are examined. The test configuration is shown in Fig. 6.

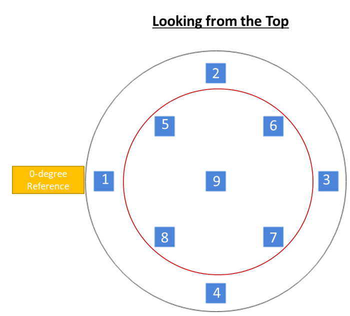

Fig. 6. Test point configuration

E. Strength Performance Metrics

The pole structural strength performance are evaluated using the the fiber strength at the rupture plane and the overall remaining strength of the pole. Each parameter is described separately below.

1) Fiber Strength and % Remaining Fiber Strength: As discussed in Section II, the stress wave is characterized by the average arrival velocity $\bar{v}_{pe}$ and the energy attenuation coefficient α_{pe}. To draw a correlation between the structural strength and the stress wave signal characteristics, the variation of different pole classes is normalized. This approach eliminates the variation introduced from different pole classes, effectively increasing the number of comparable samples for the correlation analysis.

The fiber strength measured at the break point is also compared against the designed fiber stress F_d derived from [32]. It is termed the *percentage remaining fiber* *strength* % RFS. The mathematical expression is detailed 6.

$$\%\ \text{RFS} = \frac{F_b}{F_d}, \tag{6}$$

where F_b is the measured fiber strength based on 5 and F_d is the designed fiber strength based on Table 1 in [32]. Since this metric compares the measured strength to the design strength of the specific species, it is a normalization process to estimate the level of the strength degradation.

2) Percentage Remaining Strength: The *percentage remaining strength* %RS defined by the following expression,

$$\%\ \text{RS} = \frac{P}{P_d}, \tag{7}$$

where P is the load at failure and P_d is the designed class tip load or max. load capacity. The design class tip bending capacity τ_{cap} is determined via following expression based on the ANSI 05.1 [35]:

$$\tau_{\text{cap}} = P_d L = k F_b C^3, \tag{8}$$

where k is a conversion constant (k = 0.000264). F_b is the nominal fiber strength at the ground line, and C is the ground line circumference. L is the distance between the ground line and the load point. Based on the bending capacity, the max load capacity P_d can be obtained. As noted in ANSI O5.1, this calculation contains a *coefficient of variation* (COV) of approximately 20%.

3) Average Compression Shell Strength (ACS): Based on the compression result using the method detailed in Section II-D, the assumed coordinate of the test points and the associated compression values are imported to a scatter interpolator to generate an overall response of the entire specimen. To prevent any unrealistic gradients in the overall compression response, the linear interpolator is used to produce C^0 continuity function resulting in a smooth distribution of compression results in the computational domain. To incorporate the orthotropic property of the cross-sectional plane, the proposed interpolation was performed in the polar coordinate system. The result is shown in Fig.7. The ACS Strength value is calculated using the root mean square (RMS) defined as,

$$x_{RMS} = \sqrt{\frac{1}{N}\sum_{n=1}^{N} |x_n|^2}, \tag{9}$$

where N is the number of data points, x are the compression value obtained from the linear interpolator at the selected shell region.

III. Results and Analysis

A. Model Selection and correlation analysis

This section focuses on the justification of the correlation model between the characteristics of the elastic waveform and various mechanical properties determined through the static break test. Based on the formulation produced by [17], the result suggests that the steady-state Rayleigh mode propagation is an aggregate motion of the fast and slow modes associated linearly with the phase velocity of the dilatational and distortional fields, which can be expressed as [36],

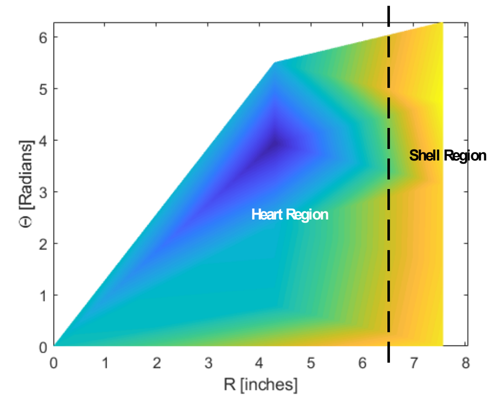

Fig. 7. Result from the linear scattered interpolator, R denotes the radial direction and θ denotes the tangential direction.

$$\begin{aligned} c_L^2 &= \frac{\lambda + 2\mu}{\rho} \\ c_T^2 &= \frac{\mu}{\rho} \end{aligned} \tag{10}$$

(10) suggests a linear relationship between the mechanical property and the velocity square. Henceforth, this model will be used to perform data fitting and correlation analysis.

Prior work conducted by [23] formulated the attenuation coefficient α of the poroelastic wave as a viscous damping term in their governing wave equation. That is,

$$\alpha = \frac{32\mu\beta}{d^2} \tag{11}$$

where μ is the fluid viscosity, β is the porosity and d is the largest linear dimension of the pores. This expression suggests that the damping ratio appears linearly with material loss. By combining the viscous damping model with the power model discussed in Section II-B2, the logarithmic model can be assumed to analyze the correlation relationship between the energy attenuation and the mechanical property.

1) Rayleigh Mode (AW2) Response to F_b: Sectional measurements using the UB1000 device are performed prior to the static break test at 0, 12, 24, 36, and 48 inches above the ground line plane. Each cross-sectional measurement is termed the plane of measurement (POM). The AW2 is then extracted according to [11], the obtained average velocity and the energy response are compared with the strength performance metrics. After the proposed static break test on the entire sample set is performed, the location of POR is measured. The poles with POR within $\pm$ 3 inches of the POM are selected. This approach assumes minimal property variation in the longitudinal direction.

23 poles used in this study due to the close proximity between the POM and POR. Within this sample set, the sample poles are from a diverse population of different species ranging from 30 feet to 55 feet. The samples are grouped based on the lengths to analyze if the age of the pole would impact the stress wave characteristics. Based on the prior discussion in Section II-B, the average velocity and the attenuation coefficient are depicted in Fig. 8. and Fig. 9. Fig. 8 compares the average propagating velocity square at the POM to the fiber strength at the POR. Using the linear regression model, the three groups 30 to 35, 40 and 50 to 55 exhibit three different correlations with the highest in 50 to 55 group. All groups suggest a directly proportional linear correlation between the average velocity and the fiber strength. The average correlation coefficient across all length groups is 0.54.

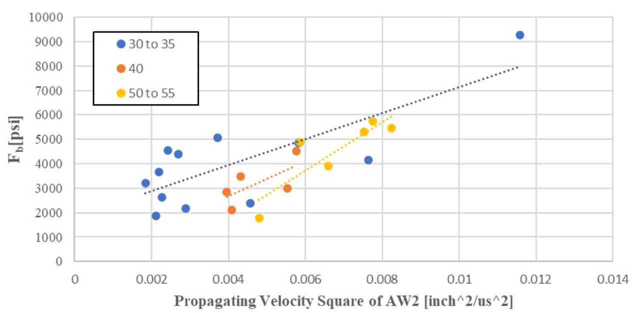

Fig. 8. Propagation Velocity square of the Rayleigh mode vs. the fiber strength at the rupture location.

Fig. 9 compares the attenuation coefficient α against the fiber strength at the POR. The energy response yields a smaller correlation coefficient compared to the average velocity depicted in Fig. 8. Two distinct clusters are formed among the three different length groups. By eliminating the spatial dependency using the power-law model, the result suggests that the larger class poles with greater groundline circumferences tend to have a smaller attenuation coefficient than the smaller class poles with smaller groundline circumference. This finding is pronounced between the length group 30 to 35 and the length group 50 to 55. By discarding the outliers, the fiber strength exhibits an inversely proportional relationship with the attenuation coefficient. This result suggests that wood fiber with a stronger fiber strength tends to have less wave energy attenuation than fiber that exhibits a weaker strength. Across all the length groups, the overall correlation coefficient is 0.1.

2) Rayleigh Mode (AW2) Response to the % Remaining Fiber Strength (RFS): The analyses of the % remaining fiber strength and AW2 response characteristics are depicted in Fig. 10 and Fig. 11. In Fig. 10, the result yields three different correlation values among the length groups. This result indicates a similar finding as Section III-A1, suggesting the correlation can be improved by individually considering each length group. The overall

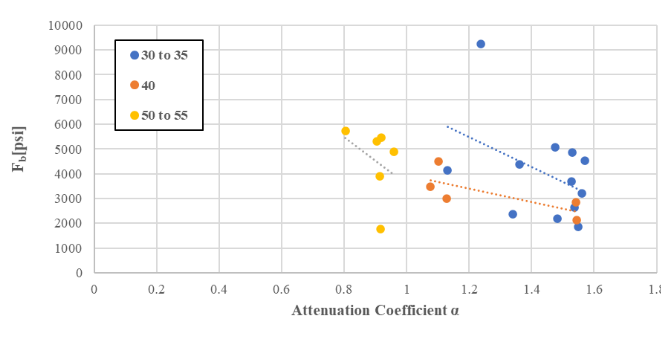

Fig. 9. Attenuation Coefficient α of AW2 vs. Fiber Strength at the Rupture Location.

correlation coefficient is 0.55, slightly stronger than the fiber strength comparison ($R^2 = 0.54$). As recalled, the % RFS based on (6) reflects the property degradation from the nominal designed strength, making this analysis technique more valuable than the fiber strength comparison.

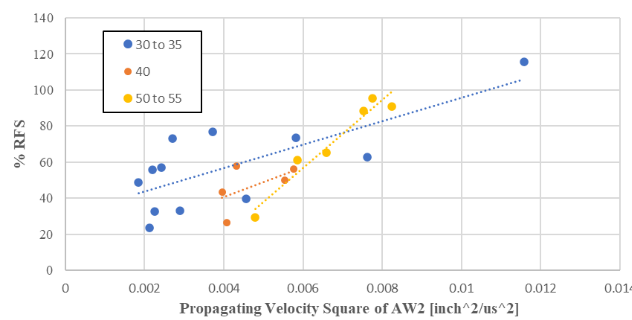

Fig. 10. Average propagation velocity Square of the Rayleigh mode vs. the % remaining fiber strength.

Fig. 11 shows two distinct clusters. The length group of 50 to 55 has a relatively lower attenuation coefficient than the length groups of 30 to 35 and 40. This finding resonates with the finding suggested in Fig. 10. This result perhaps indicates that the differences in fibril structure between the different length groups need to be considered when considering the correlation between α and %RFS. The group-specific correlation coefficients suggest that the % RFS has a higher correlation to the attenuation than the fiber strength. This result also yields an overall correlation coefficient of 0.2, a 100% increase compared to the average correlation coefficient calculated in Section III-A1. The overall inversely proportional relation indicates that the attenuation coefficient increases with decreasing %RFS. It supports the hypothesis that mechanical property degradation has a greater energy attenuation than a healthy wooden medium.

3) Rayleigh Mode (AW2) Response to the % Remaining Strength: %RS indicates the overall structural integrity at the load point based on the groundline strength assessment. Based on the strong correlation between the FB Strength and %RS (7) in Fig. **??**, This section

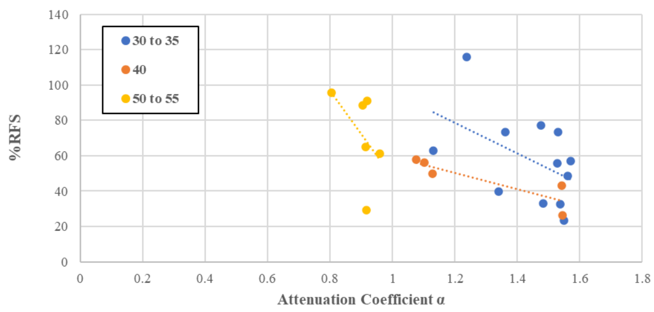

Fig. 11. Attenuation coefficient α vs. the % remaining fiber strength.

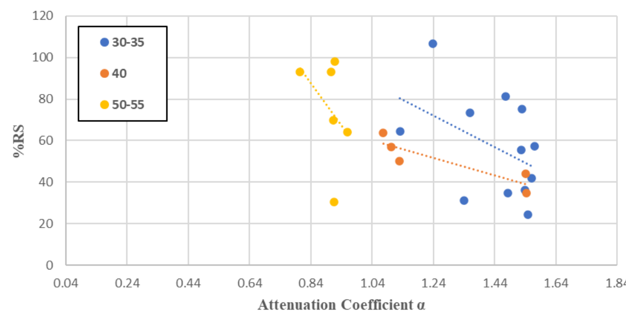

Fig. 13. Attenuation Coefficient vs. % Remaining Strength

examines a correlation between the AW2 characteristics and the % remaining strength. The related results are depicted in Fig 12 and Fig. 13. Fig. 12 compares the propagating velocity against the %RS. The R^2 resulting here indicates a slightly weaker correlation than the analyses comparing the fiber strength and the %RFS. Nevertheless, this result suggests a directly proportional relationship between the average propagating velocity and the %RS, which agrees with the analyses in Sections III-A1 and III-A2.

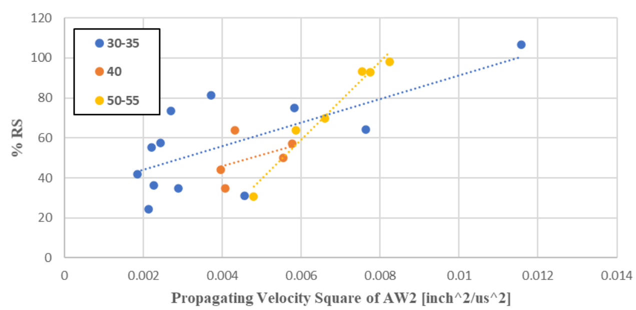

Fig. 12. Propagation Velocity of the Rayleigh mode vs. % Remaining Strength

A scatter plot between α and %RS is depicted in Fig. 13. It shows a weak correlation and a greater uncertainty between the 30-35 and 50-55 groups. However, group 40 appears to have a stronger correlation. Bear in mind that the five available data points do not warrant statistical significance. Fig. 13 shows two distinct data clusters similar to Fig. 11 and Fig. 9 between the 30-40 and 50-55 groups. The overall behavior suggests that the α increases with decreasing overall %RS.

4) Correlation Summary: Table II summarizes the correlation coefficients produced from the analyses in Section III-A1, III-A2 and III-A3. Using the different analysis techniques, the average propagating velocity of the AW2 appears to have a strong correlation among all three strength performance metrics. The velocity vs. fiber strength has the highest correlation in the length groups 30-35 and 40, but relatively weaker in the length group 40. Nevertheless, all three analyses exhibit a similar overall correlation coefficient from 0.46 to 0.49. The energy attenuation versus different strength indicators appears to be much weaker. In length group 40 however, a relatively stronger and distinct correlation of the energy response to all three strength performance metrics.

TABLE II
LINEAR AVERAGE CORRELATION COEFFICIENT OF DIFFERENT ANALYSES IN RELATION TO DIFFERENT POLE GROUPS. v AND α DENOTE THE AVERAGE PROPAGATION VELOCITY AND THE ATTENUATION COEFFICIENT RESPECTIVELY.

Analysis	30-35	40	50-55	Overall
v^2 - FB	0.62	0.47	0.75	0.54
v^2-%RFS	0.56	0.30	0.94	0.55
v^2-%RS	0.49	0.18	0.96	0.53
α - %FB	0.19	0.55	0.11	0.10
α - %RFS	0.23	0.76	0.11	0.20
α - %RS	0.20	0.79	0.16	0.23

B. Rayleigh Mode (AW2) Response to the Average Compression Shell Strength (ACS)

The section analyzes the compression test results from the procedures detailed in Section II-D and the average compression shell strength using linear scatter interpolator in the polar coordinate domain (Section II-E3). The corresponding AW2 average propagating velocity square and the average compression shell (ACS) strength values are compared in Fig. 14. Using the previous length grouping method, the analysis is repeated three times for the different pole groups (30 - 35, 40 and 50 - 55). With the assumed linear regression model, the 30 to 35 pole group exhibits the highest correlation with the approximate R^2 of 0.37. The correlation performance reduces to 0.22 and nearly 0 for pole groups of 40 and 50-55. The strong linear correlation with the directly proportional relation suggests that a greater compression strength in the shell region tends to result in a higher propagating velocity of AW2. This finding is inconsistent in larger pole groups (40 and 50 to 55), which show a weaker correlation with different proportional relations.

Using the similar approach as depicted in Fig. 14, the peak energy responses are also compared to the different pole groups. Fig. 15 shows the correlation performance of length groups 30 to 35, 40 and 50 to 55 respectively.

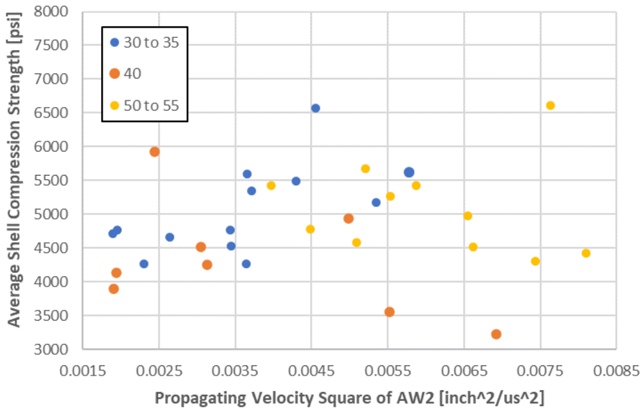

Fig. 14. Correlation between the AW2 velocity square and ACS values

Using the proposed logarithmic linear regression model, the correlation coefficients illustrate a similar finding as shown in Fig. 14 with the 30-35 exhibiting the highest correlation (R^2 = 0.38) and the R^2 values decrease with increasing in pole length. The correlation coefficient of group 30-35 indicates an inversely proportional relation, which agrees with the previous finding in Section III-A supporting the conclusion which states that the stress wave tends to have a higher attenuation coefficient in wood with a weaker ACS strength.

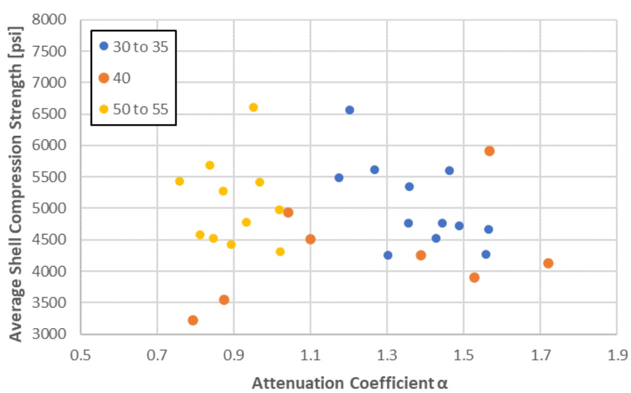

Fig. 15. Energy to compression strength correlation

Overall, the response of propagating speed and attenuation of AW2 to the ACS strength suggests a correlation if the pole length grouping method is used. A similar study was also performed when the species grouping method is used. Using the correlation coefficient as a metric of measurement, the length grouping method has a larger correlation coefficient than the species grouping method, suggesting a stronger overall dependency on the ultrasonic vs. mechanical property correlation for the length group of 30 to 35. It is worth noting that the moisture content was assumed to be the same after the specimen are exposed to the controlled environment for 43 days. Since the poles were stored horizontally before the tests, the lateral moisture due to gravitational pull might have contributed to the inhomogeneous distribution of moisture on the test surface of each specimen. The proposed linear interpolation function for calculating the ACS values can be improved using a data-driven or physics-based model in future studies.

IV. Conclusion

This study presents a comparative analysis of examining the efficacy of the ultrasonic-based NDT. This work attempts to correlate the fiber strength, the percentage remaining fiber strength, and the remaining pole strength resulting from the test with the extracted ultrasonic wave features through the standard static break test and compression testing. That is, the propagating velocity and the attenuation coefficient of the peak energy of AW2. The result produces a significant overall correlation of 0.5 between the propagating velocity and the measured pole strength. It also resulted in an acceptable correlation level of 0.2 between the peak energy level and the measured pole strength. This data-driven result allows future development of ultrasonic analysis algorithms for the pole strength calculation.

The longitudinal compression test was conducted on the cross-section surfaces. Using a linear interpolator, the average shell compression strength values were calculated to compare against the corresponding AW2 characteristics. A stronger correlation appears in the length grouping method with a smaller pole length between 30 and 35 ($R^2 \approx 0.4$). In contrast, the species groping method does not provide a conclusive result. However, the result can be improved if other interpolation schemes that are physics-driven and the contribution of moisture are included. This study reveals the efficacy of the ultrasonic-based NDT for wood pole groundline characterization. It contains significant findings for future studies of understanding the correlations at a more fundamental level.

Acknowledgment

The first author would like to thank the financial and equipment supports by the Utility Asset Mangement Inc. Denver, Colorado, and Dairyland Power Cooperative from La Crosse, Wisconsin, to provide the samples of the utility poles used in this study.

References

[1] J. E. Winandy, B. Bernhardt, D. Brooks, A. Sinha, and J. J. Morrell, “Modeling effects of incising on flexural properties of green douglas fir and western hemlock lumber,” *Journal of Testing and Evaluation*, vol. 49, no. 6, 2020.

[2] “ANSI 05. 1 wood poles,” *Specifications and Dimensions*, 2017.

[3] “Standard test methods of static tests of wood poles,” 2017.

[4] M. G. C. Uzcategui, R. D. Seale, and F. J. N. França, “Physical and mechanical properties of clear wood from red oak and white oak,” *BioResources*, vol. 15, no. 3, pp. 4960–4971, 2020.

[5] E. Fukada, “The vibrational properties of wood i,” *Journal of the Physical Society of Japan*, vol. 5, no. 5, pp. 321–327, 1950.

[6] J. Dunlop, “Damping loss in wood at mid kilohertz frequencies,” *Wood Science and Technology*, vol. 12, no. 1, pp. 49–62, 1978.

[7] V. Bucur, "An ultrasonic method for measuring the elastic constants of wood increment cores bored from living trees," *Ultrasonics*, vol. 21, no. 3, pp. 116–126, 1983.
[8] M. Suzuki and M. Suzuki, *Adsorption engineering*. Kodansha Tokyo, 1990, vol. 14.
[9] C. Senalik, "Detection and assessment of wood decay–glulam beams and wooden utility poles," Ph.D. dissertation, University of Illinois at Urbana-Champaign, 2013.
[10] R. G. Payton, "Wave fronts in wood," *The Quarterly Journal of Mechanics and Applied Mathematics*, vol. 56, no. 4, pp. 527–546, 2003.
[11] Y. Lee, "Ultrasonic-based condition assessment of wooden utility poles," 2020.
[12] J. E. Winandy and J. J. Morrell, "Relationship between incipient decay, strength, and chemical composition of douglas-fir heartwood," *Wood and Fiber Science*, vol. 25, no. 3, 1993.
[13] V. Bucur and F. Feeney, "Attenuation of ultrasound in solid wood," *Ultrasonics*, vol. 30, no. 2, pp. 76–81, 1992.
[14] H. Kim and S. W. Heo, "Time-domain calculation of spectral centroid from backscattered ultrasound signals," *IEEE transactions on ultrasonics, ferroelectrics, and frequency control*, vol. 59, no. 6, pp. 1193–1200, 2012.
[15] R. Prakash, "Non-destructive testing of composites," *Composites*, vol. 11, no. 4, pp. 217–224, 1980.
[16] M. M. Faraji, S. B. Shouraki, and E. Iranmehr, "Fuzzy based algorithm for acoustic source localization using array of microphones," in *2017 Iranian Conference on Electrical Engineering (ICEE)*. IEEE, 2017, pp. 2102–2105.
[17] Y. Lee, "Diffusive subsurface propagation of rayleigh mode induced by embedded ultrasonic waveguide," *The Journal of the Acoustical Society of America*, vol. 148, no. 4, pp. 2718–2718, 2020.
[18] Y. Lee, M. Mahoor, and W. Hall, "Rayleigh mode excitation at the half-space boundary in wood using embedded elastic waveguides," in *Proceedings of the 2019 Society of Wood Science and Technology International Convention, Tenaya Lodge, Yosemite, California, USA*. Society of Wood Science and Technology, 2019, pp. 212–219.
[19] C. A. Senalik, F. Franca, R. Seale, R. J. Ross, and R. Shmulsky, "Grading lumber with acoustic-based technologies part 2: ultimate tension stress estimation from time-and frequency-domain parameters," *Wood and Fiber Science*, vol. 52, no. 4, pp. 390–399, 2020.
[20] D. Hall, Y. Lee, and W. Hall, "Acoustic probe for inspection of wooden specimen," May 21 2020, uS Patent App. 16/518,762.
[21] Y. Lee, M. Mahoor, and W. Hall, "A 2d numerical model of ultrasonic wave propagation in wooden utility poles using embedded waveguide excitation technique," *Wood and Fiber Science*, vol. 52, no. 1, pp. 87–101, 2020.
[22] W. Shangguan, H. Ren, J. Lv, B. Fei, Z. Chen, R. Zhao, and Y. Zhao, "Cell wall property changes of white rot larch during decay process," *BioResources*, vol. 9, no. 3, pp. 4297–4310, 2014.
[23] M. Biot, "Theory of elastic waves in a fluid-saturated porous solid. 1. low frequency range," *J. Acoust. Soc. Am.*, vol. 28, pp. 168–178, 1956.
[24] Z. E. A. Fellah, M. Fellah, C. Depollier, E. Ogam, and F. G. Mitri, "Wave propagation in porous materials," *Computational and experimental studies of acoustic waves*, pp. 99–119, 2018.
[25] J. D. Achenbach and H. I. Epstein, "Dynamic interaction of a layer and a half-space," *Journal of the Engineering Mechanics Division*, vol. 93, no. 5, pp. 27–42, 1967.
[26] S. Mallat, *A wavelet tour of signal processing*. Elsevier, 1999.
[27] D. E. Newland, "Harmonic wavelets in vibrations and acoustics," *Philosophical Transactions of the Royal Society of London. Series A: Mathematical, Physical and Engineering Sciences*, vol. 357, no. 1760, pp. 2607–2625, 1999.
[28] W. K. Ngui, M. S. Leong, L. M. Hee, and A. M. Abdelrhman, "Wavelet analysis: mother wavelet selection methods," in *Applied mechanics and materials*, vol. 393. Trans Tech Publ, 2013, pp. 953–958.
[29] Y. Y. Kim and E.-H. Kim, "Effectiveness of the continuous wavelet transform in the analysis of some dispersive elastic waves," *The Journal of the Acoustical Society of America*, vol. 110, no. 1, pp. 86–94, 2001.
[30] V. Bucur and I. Böhnke, "Factors affecting ultrasonic measurements in solid wood," *Ultrasonics*, vol. 32, no. 5, pp. 385–390, 1994.
[31] P. Bajpai, *Biermann's Handbook of Pulp and Paper: Volume 1: Raw Material and Pulp Making*. Elsevier, 2018.
[32] "Ansi standard 05.1: Wood poles - specifications and dimensions," 2017.
[33] "ASTM 1036, standard test methods for static tests of wood poles," *ASTM International. West Conshohocken. PA*, 2012.
[34] "ASTM d143-21, standard test methods for small clear specimens of timber," May 21 2021.
[35] R. W. Wolfe and R. C. Moody, "Ansi pole standards: Development and maintenance," in *Proceedings of the first Southeastern pole Conference. For. Prod. Society. Madison, USA*, 1994, pp. 143–149.
[36] J. L. Rose, *Ultrasonic waves in solid media*. ASA, 2004.

Yishi Lee Dr. Yishi Lee is currently an Assistant Professor from the Metropolitan State University of Denver under the engineering and engineering technology department. His research focuses on advancing the applications of ultrasonic signal processing and analysis based on physical principles. He is also working with an industry partner specializing in ultrasonic-based stress waves for nondestructive evaluation in wooden utility poles, leading the firm in R&D and algorithmic developments. The resultant features are used for condition characterization and advance the NDE technology. His collaborative efforts with multiple government agencies, academic institutions, and private firms have helped produced numerous journal papers, conference papers, and patents.

Frederico Nistal Franca Frederico José Nistal França is an Assistant Research Professor at Mississippi State University, USA. Originally from Brazil, he holds a PhD degree in Sustainable Bioproducts from Mississippi State University (2017), aMaster degree in Forest Science (2014) and a Wood Industry Engineering degree (2012) from the Federal University of Espírito Santo, Brazil. His areas of interest are: physical and mechanical properties of wood, nondestructive evaluation of wood (NDT), modeling, heat and mass transfer during wood drying and currently, he is investigating advanced vibrational measurements as an indicator of lumber strength.

Dan Seale Dr. Dan Seale is a James R. Moreton Fellow and Thompson Professor in the Department of Sustainable Bioproducts at Mississippi State University and has advanced degrees from Mississippi State University and Clemson University. Since joining the staff in the Department of Forest Products in 1983, he has worked with many industry segments including plywood, particleboard, and oriented strand board (OSB), solid lumber including hardwood and softwood, poles and pilings, and the furniture industry. Research areas include economics, manufacturing composite wood products, product mix for plywood and OSB, and database applications tailored to individual manufacturing companies. Dr. Seale manages the mechanical testing and pressing facilities of the Department. A recent project involving Dr. Seale, Dr. Fred Franca, and Songi May Han led to the development of an IPhone application called "Smart Thumper" that is the first NDT tool that is available to consumers and capable of testing lumber utilizing longitudinal vibration and/or transverse vibration.

Jerrold E. Winandy Dr. Winandy started his own consulting firm specializing in forensic wood science, wood durability and bio-resource sustainability in 2008. He has served as an Adjunct Professor of Wood Science and Engineering at the University of Minnesota since 1998. Prior to 2008, he served for over 30 years as a Research Wood Scientist in the Engineering Properties of Wood and later as Project Leader of the Engineered Composites Science Research Units at the USDA Forest Products Laboratory in Madison WI. His research on the very early stages of thermochemical degradation and biological decay has provided insight into how changes in the chemical composition of the wood cause significant reductions in the engineering properties of wood and bio-based composites. He has authored /co-authored over 200 Technical Publications and holds two patents.

Christopher A. Senalik Dr. Senalik graduated from University of Illinois – Urbana Champaign with a focus on non-destructive testing and evaluation. In his current position as Research General Engineer for the Forest Products Laboratory in Madison, WI, he develops methods of NDE for wood based products using acoustics, stress waves, and radar.